Lithuanian Journal of Physics
Vol. **63**, No. 3, pp. 131–139 (2023)
ISSN 1648-8504 eISSN 2424-3647
DOI: https://doi.org/10.3952/physics.2023.63.3.3

VOLTAGE COTROLLED FABRY–PEROT MODULATOR

A. Kamarauskas [a], L. Staišiūnas [a], D. Seliuta [a, b], G. Šlekas [a], and Ž. Kancleris [a]

[a] *Center for Physical Sciences and Technology, Saulėtekio 3, 10257 Vilnius, Lithuania*
[b] *Vilnius Gediminas Technical University, Saulėtekio 11, 10223 Vilnius, Lithuania*
Email: andrius.kamarauskas@ftmc.lt

Received 19 September 2023; accepted 20 September 2023

Here we propose a voltage-controlled Fabry–Perot modulator made of two overlapping graphene sheets separated by a hafnium oxide layer, manufactured on a silicon substrate. The applied voltage shifts the Fermi level in both layers thus changing the total surface conductivity. This in turn changes the optical parameters of the system. Due to the architecture of the modulator, ≈50% of THz power is absorbed and the applied voltage controls the ratio between the reflection and transmittance. At the resonance frequency of 414 GHz, the transmission through the Fabry–Perot modulator can be doubly reduced in a voltage range of −1.5 to 10 V. In DC measurements, it is revealed that the electrical properties of graphene sheets dramatically depend on the technological process. The proposed multilayer structure can be manufactured on any THz-transparent substrate, compatible with photolithography and atomic layer deposition (ALD) processes. Voltage-controlled surface conductivity could find its application in sensing or modulation of electromagnetic waves.

Keywords: graphene, interference, modulation, surface conductivity
PACS: 81.05.ue, 42.25.Hz, 42.79.Hp, 73.25.+i

1. Introduction

THz is a region of electromagnetic wave spectrum that lies between microwaves and far infrared rays, with free-space wavelengths of 3 mm and 30 μm, respectively. This frequency region is relatively new and unexplored compared to other frequency ranges, opening up opportunities for innovative discoveries and technological advancements. Some of these discoveries already find applications for non-destructive testing, imaging [1] and sensing in materials science, biology [2] and security [3]. However, the development of efficient and versatile modulators capable of manipulating THz signals is still a challenge. This is where graphene-based modulators come into play. Unique properties of graphene, such as its high carrier mobility [4], tunable conductivity [5] and ultrafast response [6], make it an attractive material for THz modulation [7, 8].

For instance, surface conductivity can be modified by applying voltage to graphene strips through the ionic liquid in the periodic array of H cells [9]. The basic idea is that linking more cells modifies the properties of the array, allowing the adjustment of transmission, phase and frequency. The same principle is applied for voltage-controlled electromagnetically induced transparency (EIT) [10]. It is also possible to control surface conductivity with optical excitation. It has been demonstrated using a semi-insulating GaAs substrate, on which the laser beam and THz beam are concentrated at the same spot. Modulation of Fabry–Perot resonances is performed by sweeping the laser intensity from 0 mW (which has no effect on THz transmission) to 100 mW (which suppresses THz transmittance) [11].

In this paper, we present a novel graphene dual-layer modulator that does not require ionic gel or additional laser to modulate surface conductivity. By applying DC voltage to the graphene sheets separated by hafnium oxide, the graphene surface conductivity can be modified, thereby dynamically controlling the optical parameters (transmission/reflection) of the Fabry–Perot modulator.

2. Preparation of samples

A Fabry–Perot modulator is made on a 2 × 2 cm silicon substrate with a thickness of 525 ± 25 μm. Both sides of the silicon substrate are polished, the surface Miller index is 100, the resistivity ranges from 10000 Ωhm·cm to 1000000 Ωhm·cm. Following the RCA (*Radio Corporation of America*) cleaning steps SC1 and SC2, the samples undergo surface passivation by etching in H_2O:HF solution (100:1 by volume) for 3 min at room temperature. This etching process removes the native silicon oxide (SiO_2). As a result, the silicon dangling bonds are terminated by hydrogen atoms, resulting in a hydrophobic surface with a low surface recombination velocity [12] and an increased resistance to chemical attacks [13]. Then the etching sample is rinsed in deionized water and dried with a flow of nitrogen gas.

A 60 nm hafnium oxide layer is grown by atomic layer deposition over a period of 8 h at 175°C in a Fiji F200 ALD reactor (*Cambridge NanoTech Inc.*). Tetrakis(dimethylamino)hafnium (TDMAH, $[(CH_3)_2N]_4Hf$) with 99% purity functions as a hafnium precursor, while deionized water acts as an oxygen precursor. Argon is used as carrier gas, with a constant flow rate of 140 standard cubic centimetres per minute (SCCM) and a base pressure of ~19 Pa in the reaction chamber. A hafnium oxide layer prevents the leakage current flow in silicon, ensuring the minimal impact of environmental lighting on DC and THz measurements.

Image reversal photolithography is carried out using an AZ5214E photoresist. The photoresist is developed in H_2O:AZ351B solution (4:1 by volume) for 1 min, followed by rinsing with deionized water and drying in nitrogen gas flow. Gold contact pads are deposited by thermally evaporating Cr/Au and performing the lift-off procedure. Easy transfer graphene with PMMA poly(methyl methacrylate) on top, procured from *Graphenea, Ltd.*, is cut into 5 × 7 mm pieces. Wet transfer technique is employed to transfer graphene onto gold contact pads 1–3 (Fig. 1). Annealing of graphene is carried out by placing samples on a 120°C hotplate for 2 h. Subsequently, a combination of deep UV radiation (λ = 254 nm) and immersion in an isopropyl alcohol solution is used to remove PMMA, following the procedure described in Ref. [14].

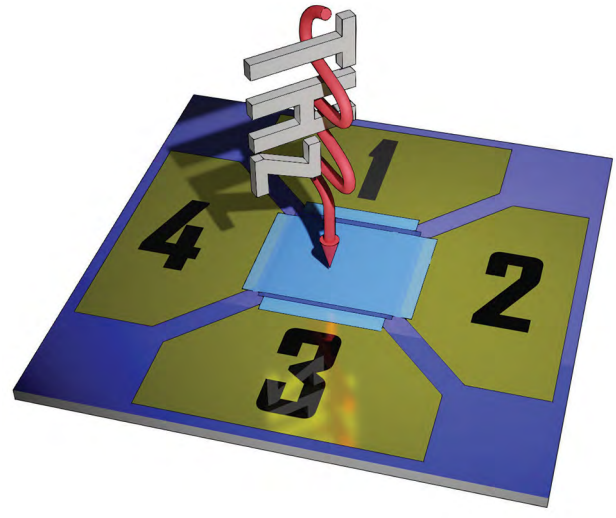

Fig. 1. A Fabry–Perot modulator features overlapping of two 5 × 7 mm graphene sheets (light blue) which are separated by 60 nm HfO_2 (dark blue). The modulator is made on a 500 μm silicon substrate (grey), and contact pads 1–4 are made of gold (yellow). A THz beam incident perpendicularly to the surface hits the overlapping part of the graphene sheets.

The second hafnium oxide layer is deposited by the ALD process described above. Before laying of the second graphene sheet, contact pads 2 and 4 were cleaned mechanically to uncover gold under hafnium oxide. Wet transfer technique is employed for placing the second 5 × 7 mm graphene sheet on pads 2–4. After the annealing, the sample is ready for measurements. The final structure of the Fabry–Perot modulator is shown in Fig. 1.

3. THz measurements

Fabry–Perot resonance can be seen in the transmission spectra of the parallel dielectric plate when waves propagate through a substrate and experience multiple internal reflections. The transmission spectrum is a periodic function of frequency with the equal spacing of high-transmittance peaks and low-transmittance dips. Transmission dips occur as a result of the destructive interference within the dielectric plate, thus part of the impinging wave is reflected back. Transmission peaks occur as a result of constructive interference within the dielectric, thus reducing reflection to the minimum. The material thickness influences the period between peaks (the highest transmission) in the frequency scale, the dielectric constant also

determines the depth of transmission dips. These spectral properties can be used for practical applications, for example, in the enhancement of antenna radiation properties [14, 15].

Experimentally, terahertz spectra are obtained using a frequency domain spectrometer *Toptica* Terascan 780. The Fabry–Perot modulator is positioned perpendicularly to the THz beam. The unpolarized beam is aimed at the intersection of two graphene sheets. Since the distance between the graphene sheets is much smaller than the THz wavelength, they act as a single unit, hence the surface conductivity of the graphene sheets is summed together. Fabry–Perot resonances are periodic, and we analyse the frequency range around a single selected Fabry–Perot peak at 414 GHz. Measurement data are obtained by sweeping frequency from 380 to 460 GHz in increments of 0.2 GHz. The transmission spectrum is calculated by dividing the data measured with the sample in the beam path by the data measured without a sample. The THz detector measures photocurrent proportional to the THz signal amplitude. Transmittance is calculated by squaring the divided THz signals. To reduce the spectrometer noise and effect of the standing waves [17], averaging and smoothing of the spectral curves is applied.

The surface conductivity of a double graphene layer, put on a dielectric slab, offers an additional degree of freedom for THz signal modulation. By applying DC voltage between the graphene layers, we are able to vary their conductivity and, in this way, the intensity of THz radiation can be modulated. The experimentally measured change of transmittance for different voltages applied to the graphene layers is shown in Fig. 2 in the vicinity of the Fabry–Perot resonance peak.

Accounting for substrate characteristics such as dielectric constant, substrate thickness and surface conductivity, one can numerically evaluate the Fabry–Perot resonance spectra of transmittance, reflectance, or absorption. Reflected wave electric field amplitudes can be written as [18]

$$E^r = -\frac{A + \mathrm{i}B\sin(k_\mathrm{d}d)}{C + \mathrm{i}D\sin(k_\mathrm{d}d)}, \tag{1}$$

where A, B, C and D are as follows:

$$A = \sigma_\mathrm{s}\eta_0\cos(k_\mathrm{d}d), \tag{2}$$

$$B = \sqrt{\varepsilon} - \frac{1}{\sqrt{\varepsilon}} + \frac{\sigma_\mathrm{s}\eta_0}{\sqrt{\varepsilon}}, \tag{3}$$

$$C = (2 + \sigma_\mathrm{s}\eta_0)\cos(k_\mathrm{d}d), \tag{4}$$

$$D = \sqrt{\varepsilon} + \frac{1}{\sqrt{\varepsilon}} + \frac{\sigma_\mathrm{s}\eta_0}{\sqrt{\varepsilon}}. \tag{5}$$

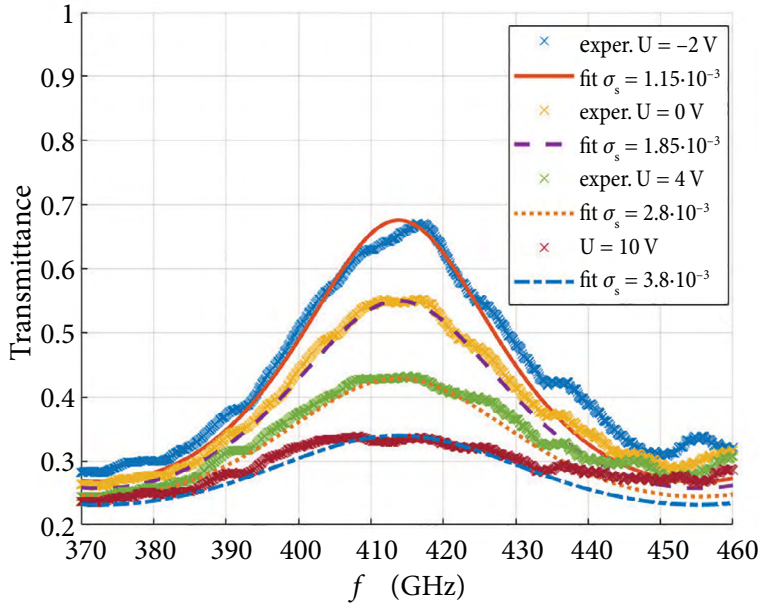

Fig. 2. Transmittance of the Fabry–Perot modulator. Symbols (x) represent measurements, other lines represent the calculated spectra with surface conductivity as a fitting parameter.

Here σ_s is the surface conductivity [S/□], ε is the relative substrate permittivity, η_0 is the impedance of free space 376.73 [Ω], d is the dielectric thickness [m], k_d denotes the wave vector amplitude in the dielectric plate, and $k_d = 2\pi\sqrt{\varepsilon}/\lambda$, λ is the wavelength in free space. The electric field amplitude for the transmitted wave is

$$E^t = \frac{2}{C + iD\sin(k_d d)}. \quad (6)$$

Having reflected and transmitted the electric field amplitude, the reflectance R and transmittance T can be expressed in the following way:

$$T = E^t \times E^{t\star}, \quad (7)$$

$$R = E^r \times E^{r\star}, \quad (8)$$

yielding the following expression for absorbance:

$$\mathcal{A} = 1 - R - T. \quad (9)$$

By varying the surface conductivity in Eq. (6), the transmittance spectra (7) are matched to the experimental data. This is shown in Fig. 2, with lines for a few selected voltages. The lowest surface conductivity corresponds to the highest THz transmittance.

The double-sided arrow at –1.5 V in Fig. 3 illustrates the range of controlled transmission and also corresponds to the Dirac's point voltage. The horizontal dashed line represents the operational voltage range of Fabry–Perot modulator. The modulation depth can be calculated from minimum and maximum transmittance values, and it determines the extent to which a carrier signal can be modulated by the applied DC voltage. As follows from the figure, by applying DC voltage the transmitted power is decreased by 50%. The modulation depth is calculated by using formula from Ref. [19],

$$MD = \frac{T_{max} - T_{min}}{T_{max} + T_{min}} \cdot 100\%, \quad (10)$$

where T_{max} is the maximum transmittance through a sample, and T_{min} is the minimum transmittance. In this particular case, the value of MD = 34% is reached.

The presence of conductive layers (graphene sheets) changes the reflection of THz radiation from the sample, leading to a change in transmission. But the calculations of absorbance using Eq. (9) reveal that transmission is significantly affected by the absorption of THz radiation in the graphene layers. It is seen in Fig. 4 that as the applied voltage changes from –1.5 to 10 V the absorbance in the graphene layers increases from 28 to 48% at 414 GHz.

The THz measurements show the combined effect of both graphene sheets. In the following section, the surface conductivity measured with THz

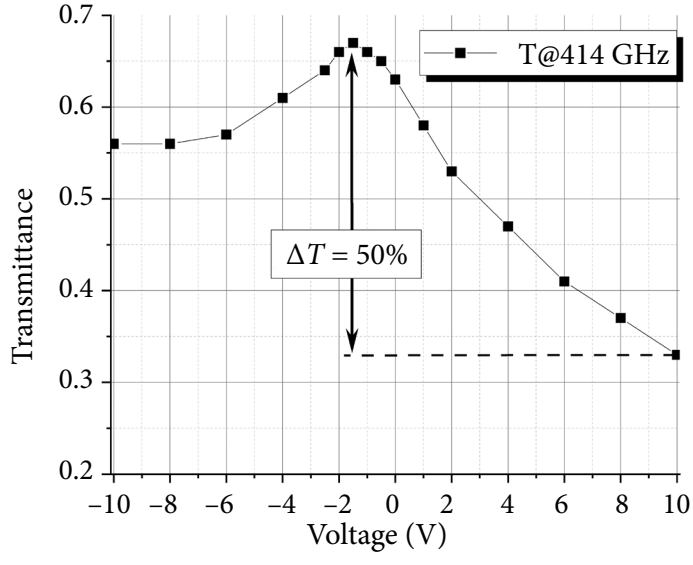

Fig. 3. Fabry–Perot modulator performance at 414 GHz. The characteristic is plotted with respect to the potential connected to the top graphene layer.

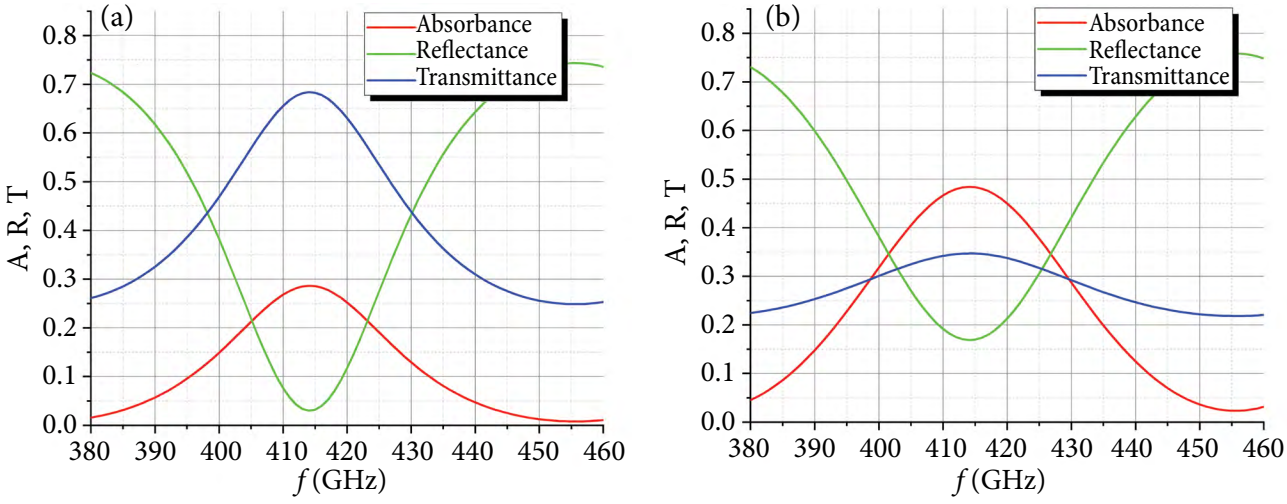

Fig. 4. Absorbance, reflectance and transmittance spectra of the Fabry–Perot modulator. Bias voltage: (a) 1.5 V and (b) 10 V. Solid lines illustrate the calculated results.

is compared with the electrical measurements using DC voltage sources and current meters. This approach provides a better understanding of the behaviour of each graphene layer.

4. DC measurements

The main factor determining the performance of the Fabry–Perot modulator is the achievable low and high surface conductivity which depends on the applied voltage and features of the graphene sheets. The conductivity of the insulating layer between the graphene sheets should be kept much lower than the conductivity of any graphene sheet to prevent the leakage current flow between the graphene sheets, which can compromise the THz modulation performance.

We repeat voltage sweep performed in the THz measurement to measure the conductivity of each layer using the voltage source U_{12}. The circuit in Fig. 5 is complemented with voltage sources U_{sh} and current meters. During the main voltage (U_{12}) sweep, the secondary voltage (U_{sh}) is kept constant at 1 V, thus simultaneously monitoring current changes in each layer. Dependent on the applied voltage the surface conductivity can be expressed in the following way:

$$\sigma_s = \frac{I_{sh}\, l}{U_{sh}\, w}. \qquad (11)$$

Here U_{sh} is the secondary voltage applied to the graphene sheet [V], I_{sh} is the current in the graphene sheet [A], w is the overlapping width of graphene sheets [m], and l is the overlapping length of graphene sheets [m].

Surface conductivity as a function of voltage between the graphene sheets is depicted in Fig. 6. Contributions of the top layer (green) and the bottom layer (light blue) to the total surface conductivity are demonstrated. The black curve corresponds to the surface conductivity obtained from the THz measurements as described in the previous section.

We observe some discrepancy between the total surface conductivity obtained from the DC measurements (red) and the conductivity obtained

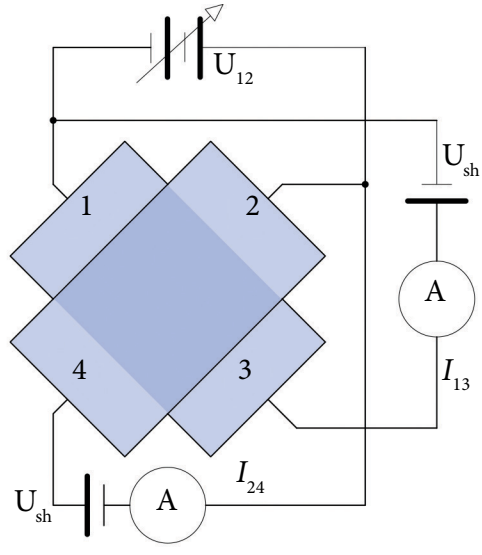

Fig. 5. Diagram for measuring graphene sheet conductivities. Voltage is applied by variable source U_{12}, currents measured for each layer are I_{13} and I_{24}, U_{sh} are the voltage sources for each layer.

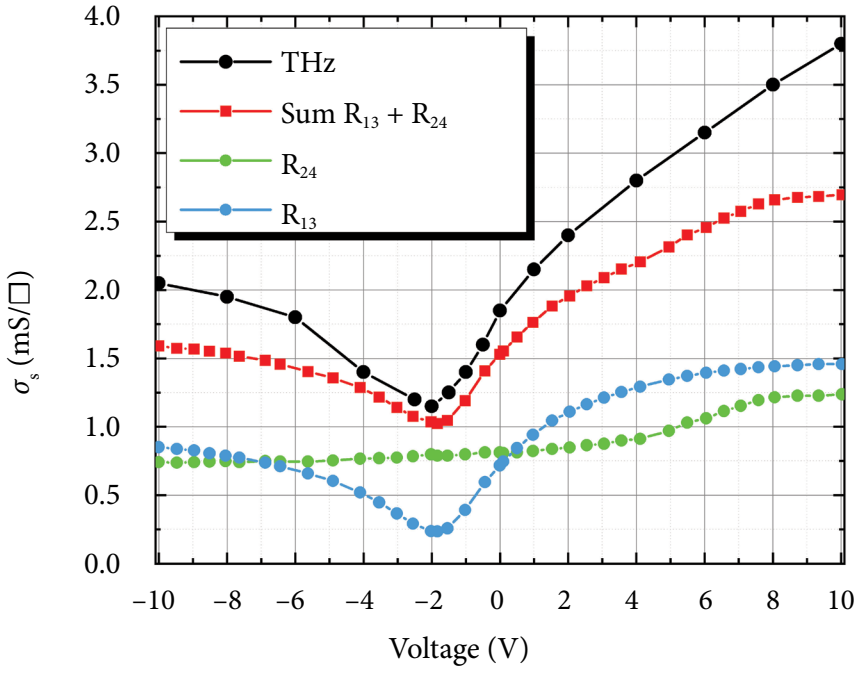

Fig. 6. Surface conductivity obtained from THz measurements (black) compared to the total surface conductivity from DC measurements (red). Other curves represent the contribution of each layer to the total surface conductivity. In the chart, a top layer voltage is referenced.

from the THz (black) across the entire voltage range. On the one hand, the contact resistance (Rc) between the graphene and gold contact pads might be present [20]. On the other hand, non-overlapping parts of graphene sheets add some additional series resistance in the DC measurements. As a result, the measured surface DC conductivity appears to be lower than the one obtained from the THz transmittance measurement.

5. Discussion of Fabry–Perot modulation performance

DC and THz measurements confirm that the voltage between the graphene sheets changes the surface conductivity of individual graphene layers, thus affecting the THz transmission through the modulator. In contrast to the THz experiment, the DC measurements allow one to analyze the contribution of each graphene layer separately. The bottom layer (R_{13}) shows a significantly higher sensitivity to the voltage change between the graphene sheets compared to that of the top layer (Fig. 6). According to the position of the Dirac's point of the bottom sheet (R_{13}), which is shifted towards negative voltages, the p-type conductivity of graphene can be determined [14, 21]. When voltage is applied, the electrostatic potential changes the charge carrier density, which causes a shift in the Fermi level [20], thus changing the conductivity of both graphene sheets. For the bottom layer (R_{13}), in the voltage interval from –10 to –1.5 V, the Fermi level is shifted out of the conduction band until the Dirac's point is reached. Here due to the ambipolar effect charge carriers change from holes to electrons. From –1.5 to 10 V, the Fermi level is shifted down towards the valence band. For the top layer (R_{24}), the Fermi level stays inside the valence band across the entire voltage range.

In our case, the p-type doping of graphene is present due to the chemicals used in PMMA removal [14]. Other doping sources might affect the modulator as well. For example, the contact between graphene and physisorptive metals like Al, Cu, Ag, Au and Pt can change the Fermi level locally and affect the concentration of electrons and holes [22]. It is reported that the carbon nanotube conductivity significantly changes when nanotubes are exposed to a mixture of Ar, NH_3, NO_2 and air [15]. In another instance, the report by Krüger [23] discovered that covering a carbon nanotube sample with aqueous solutions of $LiClO_4$,

$KMnO_4$ and H_3PO_3 shifted the Dirac's point. There is also possible to create more than one Dirac's point either due to local gates or the p-n junction formed by chemical doping. This phenomenon is explained in the article on graphene and MoS_2 overlapping sheets [24].

Here, we demonstrate a voltage-controlled surface conductivity that provides the dynamic control of THz power in an otherwise static system. This feature could be very useful for more advanced resonant structures, like metasurfaces where Fano resonances are observed. Multiple Fano resonances are demonstrated in an array of split ring resonators (SRR) on a low loss dielectric (PTFE) [25]. This resonance is very sensitive to changes in surface conductivity and dielectric loss. It is considered to combine Fano resonance and voltage-controlled surface conductivity. Furthermore, due to the excellent mechanical properties of graphene, our work can be extended to develop and optimize graphene-based modulators on thin flexible polymer substrates to create multilayer non-planar metamaterial devices operating at terahertz frequencies.

By purposefully engineering multiple Dirac's points it is possible to create logic gates [26], or use the concept in aqueous solution sensors. Another improvement in the modulator performance is expected from advanced technological processes and a broader selection of materials. For example, the Dirac's point can be shifted to lower voltages during annealing in the He atmosphere by applying voltage to remove ambient contamination by Joule heating [27]. The use of this technique would reduce the control voltage range.

6. Conclusions

We demonstrated the voltage-controlled Fabry–Perot modulator based on the mutual gating of two graphene sheets separated by a hafnium oxide layer deposited on a silicon substrate. The working principles have been highlighted, indicating that voltage shifts the Fermi level in both graphene sheets, thus affecting the total surface conductivity more than 3 times. This in turn determines the optical parameters of the Fabry–Perot modulator. In a voltage range of –1.5 to 10 V, the ratio between reflectance and transmittance is controlled, thus resulting in the modulation depth of 34%. THz and DC measurements allow one to estimate the Dirac's point position and quantitatively evaluate surface conductivity. We observe that the behaviour of graphene layer conductivity strongly depends on the chemicals used for processing. The proposed modulator can be made on any mechanically stable dielectric surface compatible with processes of photolithography and ALD. It can be applied for sensing or modulation at terahertz frequencies.

References

[1] F. Ellrich, M. Bauer, N. Schreiner, A. Keil, T. Pfeiffer, J. Klier, S. Weber, J. Jonuscheit, F. Friederich, and D. Molter, Terahertz quality inspection for automotive and aviation industries, J. Infrared Millim. Terahertz Waves **41**(4), 470–489 (2020), https://doi.org/10.1007/s10762-019-00639-4

[2] S.H. Lee, J.H. Choe, C. Kim, S. Bae, J.S. Kim, Q.H. Park, and M. Seo, Graphene assisted terahertz metamaterials for sensitive bio-sensing, Sens. Actuators B Chem. **310**, 127841 (2020), https://doi.org/10.1016/j.snb.2020.127841

[3] T. Ikari, Y. Sasaki, and C. Otani, 275–305 GHz FM-CW Radar 3D imaging for walk-through security body scanner, Photonics **10**(3), 343 (2023), https://doi.org/10.3390/photonics10030343

[4] M.A. Andersson, Y. Zhang, and J. Stake, A 185-215-GHz subharmonic resistive graphene FET integrated mixer on silicon, IEEE Trans. Microw. Theory Tech. **65**(1), 165–172 (2017), https://doi.org/10.1109/TMTT.2016.2615928

[5] A. Ahmadivand, B. Gerislioglu, and Z. Ramezani, Gated graphene island-enabled tunable charge transfer plasmon terahertz metamodulator, Nanoscale **11**(17), 8091–8095 (2019), https://doi.org/10.1039/c8nr10151e

[6] L. Viti, A.R. Cadore, X. Yang, A. Vorobiev, J.E. Muench, K. Watanabe, T. Taniguchi, J. Stake, A.C. Ferrari, and M.S. Vitiello, Thermoelectric graphene photodetectors with sub-nanosecond response times at terahertz frequencies, Front. Opt. Photonics **10**(1), 89–98 (2021), https://doi.org/10.1515/9783110710687-007

[7] C. In, H.D. Kim, B. Min, and H. Choi, Photoinduced nonlinear mixing of terahertz dipole resonances in graphene metadevices, Adv.

Mater. **28**(7), 1495–1500 (2016), https://doi.org/10.1002/adma.201504444

[8] S.H. Lee, H.D. Kim, H.J. Choi, B. Kang, Y.R. Cho, and B. Min, Broadband modulation of terahertz waves with non-resonant graphene metadevices, IEEE Trans. Terahertz Sci. Technol. **3**(6), 764–771 (2013), https://doi.org/10.1109/TTHZ.2013.2285615

[9] H. Jung, J. Koo, E. Heo, B. Cho, C. In, W. Lee, H. Jo, J.H. Cho, H. Choi, M.S. Kang, and H. Lee, Electrically controllable molecularization of terahertz meta-atoms, Adv. Mater. **30**(31), 1–7 (2018), https://doi.org/10.1002/adma.201802760

[10] H. Jung, H. Jo, W. Lee, B. Kim, H. Choi, M.S. Kang, and H. Lee, Electrical control of electromagnetically induced transparency by terahertz metamaterial funneling, Adv. Opt. Mater. **7**(2), 1–6 (2019), https://doi.org/10.1002/adom.201801205

[11] G. Šlekas, D. Seliuta, J. Devenson, A. Urbanovič, and Kancleris, Modulation of terahertz radiation using optical control of Fabry–Perot resonances, Electron. Lett. **51**(23), 1908–1909 (2015), https://doi.org/10.1049/el.2015.2396

[12] E. Yablonovitch, D.L. Allara, C.C. Chang, T. Gmitter, and T.B. Bright, Unusually low surface-recombination velocity on silicon and germanium surfaces, Phys. Rev. Lett. **57**, 249 (1986).

[13] W. Kern, *Handbook of Semiconductor Wafer Cleaning Technology: Science, Technology, and Applications* (Noyes Publications, Westwood, New Jersey, 1993).

[14] J. Jorudas, D. Pashnev, I. Kašalynas, I. Ignatjev, G. Niaura, A. Selskis, V. Astachov, and N. Alexeeva, Green removal of DUV-polarity-modified PMMA for wet transfer of CVD graphene, Nanomaterials **12**(22), 1–17 (2022), https://doi.org/10.3390/nano12224017

[15] J. Kong, N.R. Franklin, C. Zhou, M.G. Chapline, S. Peng, K. Cho, and H. Dai, Nanotube molecular wires as chemical sensors, Science **287**(5453), 622–625 (2000), https://doi.org/10.1126/science.287.5453.622

[16] B. Aqlan, M. Himdi, H. Vettikalladi, and L. LeCoq, A 300-GHz low-cost high-gain fully metallic Fabry–Perot cavity antenna for 6G terahertz wireless communications, Sci. Rep. **11**(1), 1–9 (2021), https://doi.org/10.1038/s41598-021-87076-3

[17] A. Roggenbuck, K. Thirunavukkuarasu, H. Schmitz, J. Marx, A. Deninger, I.C. Mayorga, R. Güsten, J. Hemberger, and M. Grüninger, Using a fiber stretcher as a fast phase modulator in a continuous wave terahertz spectrometer, J. Opt. Soc. Am. B. **29**(4), 614 (2012), https://doi.org/10.1364/josab.29.000614

[18] P. Ragulis, R. Simniškis, and Ž. Kancleris, Shift and elimination of microwave Fabry-Perot resonances in a dielectric covered with a thin metal layer, J. Appl. Phys. **117**(16), 163101 (2015), https://doi.org/10.1063/1.4918917

[19] G.D. Boreman and E.R. Raudenbush, Modulation depth characteristics of a liquid crystal television spatial light modulator, Appl. Opt. **27**(14), 2940 (1988), https://doi.org/10.1364/ao.27.002940

[20] A. Das, S. Pisana, B. Chakraborty, S. Piscanec, S.K. Saha, U.V. Waghmare, K.S. Novoselov, H.R. Krishnamurthy, A.K. Geim, A.C. Ferrari, and A.K. Sood, Monitoring dopants by Raman scattering in an electrochemically top-gated graphene transistor, Nat. Nanotechnol. **3**(4), 210–215 (2008), https://doi.org/10.1038/nnano.2008.67

[21] P. Joshi, H.E. Romero, A.T. Neal, V.K. Toutam, and S.A. Tadigadapa, Intrinsic doping and gate hysteresis in graphene field effect devices fabricated on SiO_2 substrates, J. Phys. Condens. Matter. **22**(33), 334214 (2010), https://doi.org/10.1088/0953-8984/22/33/334214

[22] A. Sakavičius, *Nanometrinio storio sluoksniuotų darinių su grafenu savybių priklausomybė nuo konstrukcijos ir aplinkos poveikio* (Dependence of the properties of the nanometer-thin layered structures containing graphene on the layout and the ambient conditions), Doctoral Thesis (Vilnius University, Lithuania, 2021), https://doi.org/10.15388/vu.thesis.149 [in Lithuanian].

[23] M. Krüger, I. Widmer, T. Nussbaumer, M. Buitelaar, and C. Schönenberger, Sensitivity of single multiwalled carbon nanotubes to the environment, New J. Phys. **5**, 1–11 (2003), https: //doi.org/10.1088/1367-2630/5/1/138

[24] S. Rathi, I. Lee, D. Lim, J. Wang, Y. Ochiai, N. Aoki, K. Watanabe, T. Taniguchi, G.-H. Lee, Y.-J. Yu, P. Kim, and G.-H. Kim, Tunable electrical and optical characteristics in monolayer graphene and few-layer MoS_2 heterostructure devices, Nano Lett. **15**(8), 5017–5024 (2015), https://doi.org/10.1021/acs.nanolett.5b01030

[25] A. Kamarauskas, D. Seliuta, G. Šlekas, M. Sadauskas, E. Kvietkauskas, R. Trusovas, K. Ratautas, and Ž. Kancleris, Experimental demonstration of multiple Fano resonances in a mirrored array of split-ring resonators on a thick substrate, Sci. Rep. **12**(1), 1–9 (2022), https://doi.org/10.1038/s41598-022-20434-x

[26] R. Sordan, F. Traversi, and V. Russo, Logic gates with a single graphene transistor, Appl. Phys. Lett. **94**(7), 1–3 (2009), https://doi.org/10.1063/1.3079663

[27] F. Traversi, V. Russo, and R. Sordan, Integrated complementary graphene inverter, Appl. Phys. Lett. **94**(22), 1–4 (2009), https://doi.org/10.1063/1.3148342

ĮTAMPA VALDOMAS FABRY IR PEROT MODULIATORIUS

A. Kamarauskas [a], L. Staišiūnas [a], D. Seliuta [a, b], G. Šlekas [a], Ž. Kancleris [a]

[a] *Fizinių ir technologijos mokslų centras, Vilnius, Lietuva*

[b] *VILNIUS TECH, Vilnius, Lietuva*

Santrauka

Pagamintas ir ištirtas įtampa valdomas Fabry ir Perot moduliatorius, ant silicio padėklo klojant du grafeno sluoksnius ir juos atskiriant hafnio oksidu (HfO_2). Prijungus įtampą tarp grafeno sluoksnių abiejuose sluoksniuose ji skirtingai paveikia Fermi lygio padėtį, todėl keičiasi bendras paviršiaus laidumas. Tai keičia visos sistemos optinius parametrus. Dėl moduliatoriaus architektūros beveik 50 % galios sugeriama grafeno sluoksnyje. Įtampa valdomas santykis tarp atspindėtos ir praėjusios bangos per Fabry ir Perot moduliatorių. Nustačius 414 GHz rezonansinį dažnį, praėjusį elektromagnetinės bangos galingumą galima sumažinti du kartus įtampos diapazone nuo –1,5 iki 10 V. Atlikus nuolatinės srovės (DC) matavimus paaiškėjo, kad grafeno sluoksnių elektrinės savybės labai priklauso nuo technologinio proceso. Šią daugiasluoksnę struktūrą galima pagaminti ant bet kokio THz bangoms skaidraus pagrindo, suderinamo su fotolitografija bei atominio sluoksnio nusodinimo (ALD) technologija. Įtampa valdomas paviršiaus laidumas galėtų būti naudingas elektromagnetinių bangų jutikliams ar moduliatoriams.